INFORMATICS JOURNALS

ISSN (Print) : 0013-466X
ISSN (Online) : xxxx-xxxx

The Journal of Electrochemical Society of India, Volume 75, Issue (2), April-June 2026; pp. 149-157

DOI: 10.18311/JESCI/2026/56333

Electrophoretically Modified 316L Stainless Steel: A Promising Approach for Durable and Biocompatible Bone Implants

K. Aruna, R. Vignesh, P. V. Benisha and T. M. Sridhar*

Department of Analytical Chemistry, University of Madras, Guindy Campus, Chennai - 600025, Tamil Nadu, India

Abstract

Implant failures often stem from poor osseointegration, electrochemical manifestations, and infections. This research addressed these challenges by developing a bioceramic-based composite coating for Stainless Steel (316L SS), aiming to prevent the release of toxic metal ions in the body. Nano-hydroxyapatite (nHAP) was synthesised using a wet chemical precipitation method, while Graphene Oxide (GO) was prepared via a modified Hummers' method. A 99:1 nHAP-GO composite was then created using an ex-situ method. Both nHAP and the 99:1 nHAP-GO composite were coated onto 316L SS substrates through Electrophoretic Deposition (EPD), utilising isopropanol as the solvent. Characterisation techniques such as Fourier transform infrared (FTIR) and X-ray Diffraction (XRD) confirmed the presence of functional groups, phase purity, and the crystalline nature of the synthesised and prepared samples. Atomic Force Microscopy (AFM) analysis revealed that the coated samples had increased roughness compared to bare 316LSS. This enhanced roughness is beneficial, as it promotes a better osseointegration process for the coated implants. Crucially, electrochemical studies demonstrated significantly higher corrosion resistance for the composite-coated 316LSS when compared to both nHAP-coated 316LSS and bare 316LSS.

Keywords: Corrosion Resistance, Electrophoretic Deposition, Graphene, 316L SS (Stainless Steel)

1. Introduction

Researchers worldwide have dedicated significant efforts to develop metallic implants that pose no serious issues to the human body. Due to increasing demands in internal fracture fixation and bone repair, various types of metals and their alloys are commonly used in orthopedic implants[1]. These implants must exhibit high resistance to corrosion and wear when exposed to bodily fluids. Furthermore, they should not trigger any allergic reactions in surrounding tissues and must possess excellent fracture toughness[2]. Commonly used orthopaedic implants include 316L Stainless Steel (316LSS), cobalt-based (Co-Cr) alloys, and titanium and its alloys. 316LSS is widely chosen for orthopaedic implants due to its affordability, ease of fabrication, and respectable corrosion resistance[3]. It has seen extensive use in both long-term implants like total hip replacements and temporary implants such as screws and hip nails[4-6]. Despite its reasonable corrosion resistance, prolonged exposure to the body can, in the long term, lead to the release of toxic elements like nickel and chromium from 316LSS, which can damage organs like the kidneys and liver, as well as blood cells. To mitigate the release of these toxic metals, surface modification is a promising approach to significantly enhance the corrosion resistance of these metallic implants[7].

*Author for correspondence

*Email: tmsridhar23@gmail.com

Surface modification of 316LSS can be achieved by applying coatings using biocompatible bioceramics. Nano-hydroxyapatite (nHAP), with the chemical formula $Ca_{10}(PO_4)_6(OH)_2$, is a prominent bioceramic widely used for orthopaedic implant coatings[8]. Its primary advantage stems from its chemical composition closely mirroring the inorganic compounds found in human bone[9-11]. Beyond this compositional similarity, nHAP is also highly biocompatible and possesses excellent osseointegration properties. However, nHAP does have limitations, including low mechanical strength, poor load-bearing capacity, and brittleness[12].

Therefore, to enhance its physical properties, nHAP can be deposited as composites[13]. GO can be incorporated as a nanofiller into nHAP, as GO's excellent mechanical strength and antibacterial properties have recently made it a popular choice for biomedical applications[14-18]. Its antibacterial nature helps eliminate pathogen growth on orthopaedic implant surfaces. Thus, nHAP-GO composite coatings on orthopaedic implants can produce bioactive surfaces with enhanced corrosion protection. Various methods exist for applying biocomposites to 316LSS, including Electrophoretic Deposition (EPD), Laser Melting (LSM), Laser Alloying (LSA), ion beam, Physical Vapour Deposition (PVD), and the Sol-gel method. Among these, Electrophoretic Deposition (EPD) was selected for coating composite ceramics, thin films, and carbon nanotubes because of its simplicity, cost-effectiveness, applicability to large volumes and sizes, and ability to form homogeneous, uniform coatings even on complex structures[19,20]. Based on the literature survey, HAP/GO composite coatings have been investigated for deposition on stainless steel substrates, particularly for improving corrosion resistance and their potential use in orthopaedic implant applications. However, limited studies have focused on the use of n-HAP/GO and its deposition on 316L stainless steel using the EPD technique, as the major issues are with the addition of GO up to 12 %[21,22]. The major problems with EPD are that the addition of GO and HAP usually results in the formation of clumps in liquids and uneven deposit distribution on the electrodes. Hence, in the present study, the bath was formulated to have nHAP and GO composites in the ratio 99:1, and further conditions were optimised for deposition at 70 V for 1 minute. Therefore, the novelty of this work lies in the combination of the optimised n-HAP/GO composition and EPD parameters for depositing and evaluating the surface and corrosion properties of the coating for potential orthopaedic implant applications.

2. Experimental procedure

2.1 Synthesis of nHAP, GO and Preparation of nHAP-GO Composites

nHAP was synthesised via the wet chemical precipitation method. To the 1M Calcium nitrate, 0.1 M Cetyltrimethylammonium Bromide Surfactant (CTAB) was added and stirred well. To this mixture $(NH_4)_2HPO_4$ was added, and the pH was maintained at 10-11. Then the solution was left overnight for ageing. The precipitate was filtered, dried and sintered. GO was synthesised by the modified Hummers' method, where graphite, $NaNO_3$ and conc.H_2SO_4 were used as precursors and magnetically stirred to mix well. The solution was kept in an ice bath, and $KMnO_4$ was added slowly to the mixture and then allowed to stir. H_2O_2 was added dropwise and again stirred well. Then the above mixture was neutralised with water. Using 5% HCl and ethanol, the GO was centrifuged, and the precipitate was dried in an oven at 100^0C.

nHAP and GO composites were prepared by *the ex-situ* method in the ratio 99:1 using double-distilled water. Both nHAP and GO were separately sonicated for 30 mins and stirred separately. GO colloidal solution was transferred to the nHAP solution and then allowed to stir until a homogeneous mixture was obtained. The composite was obtained by centrifuging and then air-dried. The synthesised and prepared samples were then characterised by FTIR (Bruker Tensor 27) to confirm the presence of functional groups, and the samples' purity and crystallinity were confirmed by XRD (Rigaku Ultima IV).

2.2 Material Preparation for Electrophoretic Deposition

Nano-hydroxyapatite (nHAP) and GO as a 99:1 nHAP-GO composite were coated onto 316LSS substrates using electrophoretic deposition. 316LSS samples were cut to dimensions of 2 ×2 (cm) ×2 (mm) (length × width × thickness) and sequentially polished with 150, 220, 400, 600, and 800-grade SiC papers. Following polishing, the samples were degreased with acetone, rinsed with water, and then oven-dried. One side of each 316LSS sample was subsequently masked with Teflon tape. A 304 SS electrode, prepared using the same cleaning procedure, served as the anode.

To prepare the coating bath, a 2.5% nHAP-GO composite was dispersed in isopropyl alcohol and stirred for 24 hours. The dispersion was then sonicated for 30 minutes. Electrophoretic Deposition (EPD) was performed by placing the anode and cathode 1 cm apart, with the deposition occurring on a 2cm² surface area of the 316LSS samples. The samples were coated at 70V for 1 minute. After coating, the surface topography and roughness of both the bare and coated samples were analysed using AFM.

2.3 Electrochemical Studies

Electrochemical measurements were done to determine the corrosion resistance of the Bare 316LSS, nHAP and 99:1 nHAP-GO-coated 316LSS. The electrochemical studies were carried out using Ringer's solution, which was prepared using 8.6 g/L NaCl, 0.33g/L $CaCl_2$, 0.3g/L KCl and 0.2g/L $NaHCO_3$ at pH 7.4 and room temperature. This study involved Open Circuit Potential (OCP) vs Time measurements, Electrochemical Impedance Spectroscopy (EIS), and Potentiodynamic studies (Tafel Plot). All electrochemical experiments were conducted using a three-electrode flat-bottom corrosion cell with a PARSAT PMC 2000A electrochemical workstation under ambient conditions. The bare and coated samples served as the working electrode, a saturated calomel electrode was used as the reference electrode, and a graphite rod acted as the counter electrode. A 1cm² sample area was exposed to Ringer's solution for the duration of the study. Both bare and coated samples were immersed in Ringer's solution for 30 minutes while their OCP was monitored.

3. Results and Discussion

3.1 Analysis of Phase Purity of the Samples by XRD

XRD analysis was used to determine the phases and purity of the samples, providing insight into their crystalline and amorphous natures. Figure 1 represents the XRD diffractograms for nHAP, GO, and 99:1 nHAP-GO composites. The XRD peaks confirmed the crystalline nature of nHAP, while GO exhibited an amorphous nature. Importantly, the intrusion of GO into nHAP did not alter its phase purity or crystalline structure. The diffraction peaks for nHAP were observed at 2θ angles of approximately 26°, 31.9°, 33°, 40°, 46.89°, and 49.65°, corresponding to the crystal planes (002), (211), (112), (202), (222), and (213), respectively. These peaks confirm nHAP's hexagonal phases and crystallinity. In contrast, the XRD pattern for GO showed only two diffraction peaks, at 10.92° (001) and 42.68° (111), which indicates its amorphous nature. All diffraction peaks assigned to nHAP, GO, and the 99:1 nHAP-GO composite were consistent with JCPDS card no. 09-0432[23,24].

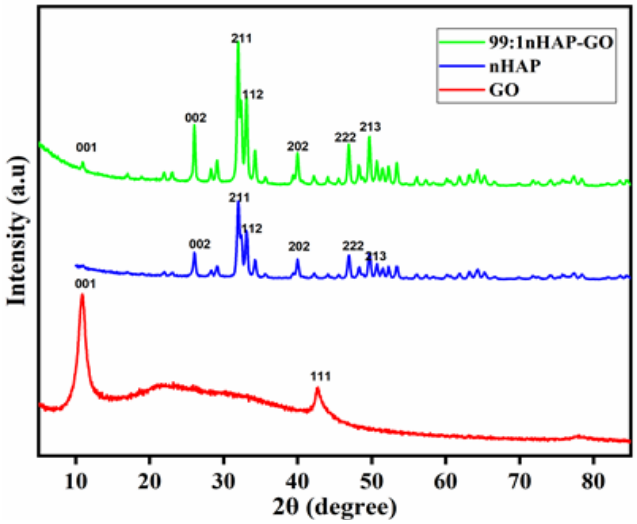


Figure 1. XRD spectra of nHAP, GO and 99:1nHAP-GO composite.

3.2 Detection of Functional Groups by Fourier Transform Infrared Analysis

Figure 2 displays the FTIR spectra, which confirm the presence of key functional groups in the synthesised nHAP, GO, and the prepared 99:1 nHAP-GO composites. The FTIR spectrum for GO shows peaks at 3399cm^{-1} (due to O-H stretching), 1722cm^{-1} (C=O), 1603 cm ^{1} (C=C), and 1022cm^{-1} (C-O linkages). For both nHAP and the nHAP-GO composite, intense peaks were observed at 1098cm^{-1} and 1020cm^{-1}, which are critical peaks attributed to the symmetric vibrations of the phosphate group (PO_4^{3-}). The spectrum at 961cm^{-1} corresponds to the asymmetric stretching vibrations of the PO_4^{3-} group. Peaks at 607cm^{-1} and 561cm^{-1} are due to the triply degenerate bending vibrations of the PO_4^{3-} group, and a 470cm^{-1} peak also indicates the presence of bending vibrations of PO_4^{3-}. The presence of these distinct stretching and bending modes of the phosphate group is crucial, confirming the successful formation of nHAP[25].

3.3 Atomic Force Microscopy Analysis

AFM provides insights into the surface topography and particle size within composites, as well as the roughness values of both bare and coated 316LSS. Figure 3 presents three-dimensional surface topography images of (a) Bare 316LSS, (b) nHAP-coated 316LSS, and (c) 99:1 nHAP-GO-coated 316LSS. The image of the bare 316LSS surface clearly shows that it has less roughness compared to the coated samples. Increased surface roughness generally enhances the bonding between bone and implant, which in turn boosts its bioactivity. The Root Mean Square (RMS) surface roughness values (Ra) were determined to be 10.252nm for bare 316LSS, 87.373nm for nHAP-coated 316LSS, and 108.355nm for 99:1 nHAP-GO-coated 316LSS. The notable increase in roughness values for the coated samples is beneficial as it promotes the osseointegration process once implanted[26].

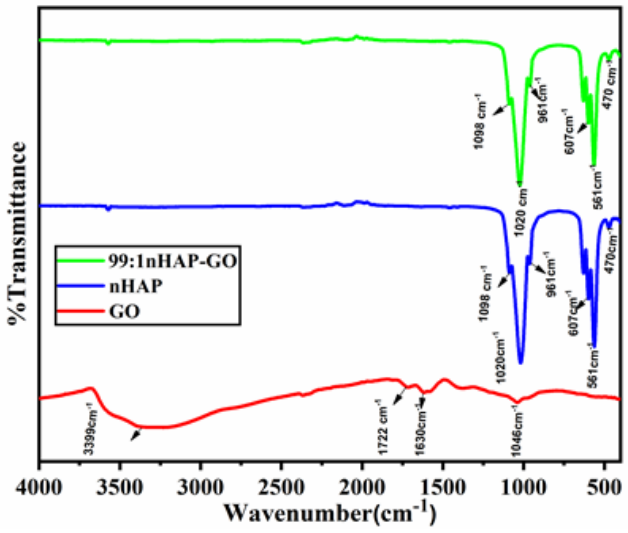


Figure 2. FTIR spectrum for GO, nHAP and 99:1nHAP-GO composite.

3.4 Electrochemical Corrosion Studies

Figure 4 presents the OCP vs time measurements for bare 316LSS, nHAP-coated 316LSS, and 99:1 nHAP-GO-coated 316LSS. Their respective OCP values were recorded as -0.789V, -0.645V, and -0.012V. The OCP value for bare 316LSS shifted towards a more active (negative) region, while the values for both coated 316LSS samples shifted towards a more positive direction when compared to the bare 316LSS. This positive shift indicates improved corrosion resistance of the coated samples. Notably, the composite (99:1 nHAP-GO) coatings exhibited a greater positive shift than the nHAP coatings, suggesting superior corrosion resistance.

EIS studies were conducted in Ringer's solution to assess the corrosive nature of the metals. A frequency sweep from 10 kHz to 0.01 Hz with an amplitude of 10mV was applied. The resulting Nyquist impedance values were then fitted using Zimpwin software for analysis. The fitted Nyquist plot is presented in Figure 5(a). Based on the simulated values, the equivalent circuit for both bare and coated 316LSS is shown in Figure 6. For bare 316LSS, Rs represents the solution resistance, R_2 is the polarisation resistance of the metal surface, and C denotes the double-layer capacitance of the metal surface. For coated samples, Rs still represents the solution resistance. However, R_1 signifies the polarisation resistance of the coated layer, Q_1 is the constant phase element of the coated layer, and R_2 remains the polarisation resistance of the metal surface.

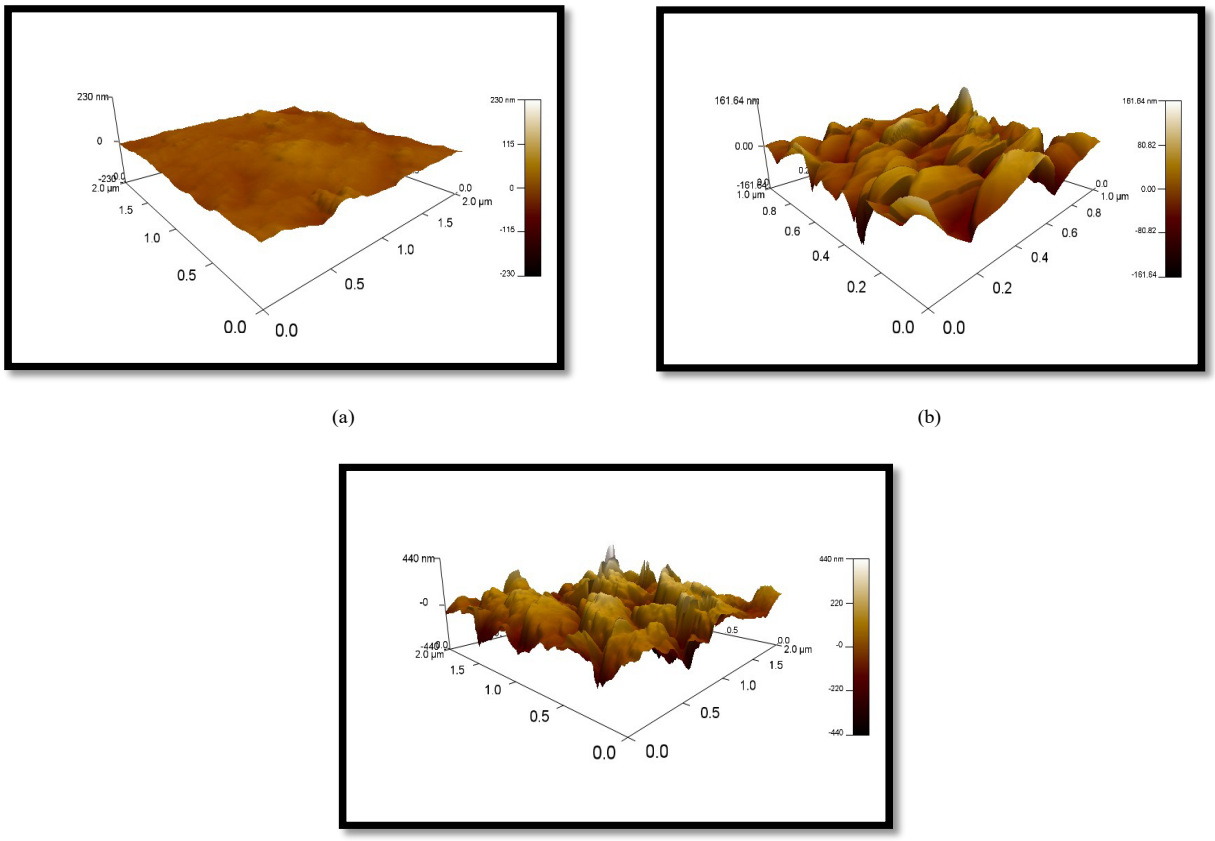


Figure 3. 3D AFM images of **(a)** Bare 316LSS, **(b)** nHAP-coated 316LSS and **(c)** 99:1nHAP-GO coated 316LSS.

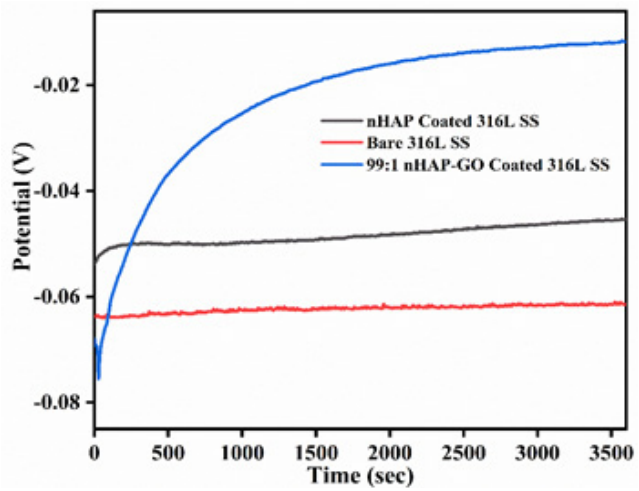


Figure 4. Open–circuit potential–time measurement of bare 316LSS, nHAP and 99:1nHAP-GO coated 316LSS in Ringer's solution.

All these values are provided in Table 1. The 'n' value, which falls within the range of 0.7 to 0.85, indicates the ability of both bare and coated samples to protect the layer from corrosion. A lower 'n' value suggests better corrosion resistance. Here, the 99:1 nHAP-GO coated sample exhibits a lower 'n' value, implying superior corrosion resistance. Additionally, the coated samples generally display a higher impedance value (|Z|). The resistance of coated samples increased with an increase in the |Z| value and a decrease in the capacitance value. When compared with the composite coating with nHAP coating, composite coatings possess high impedance, resistance and low capacitance values, which makes them better corrosion resistant.

Bode impedance and Bode phase angle plots were given in Figures 5 (b) and (c). Bode impedance values

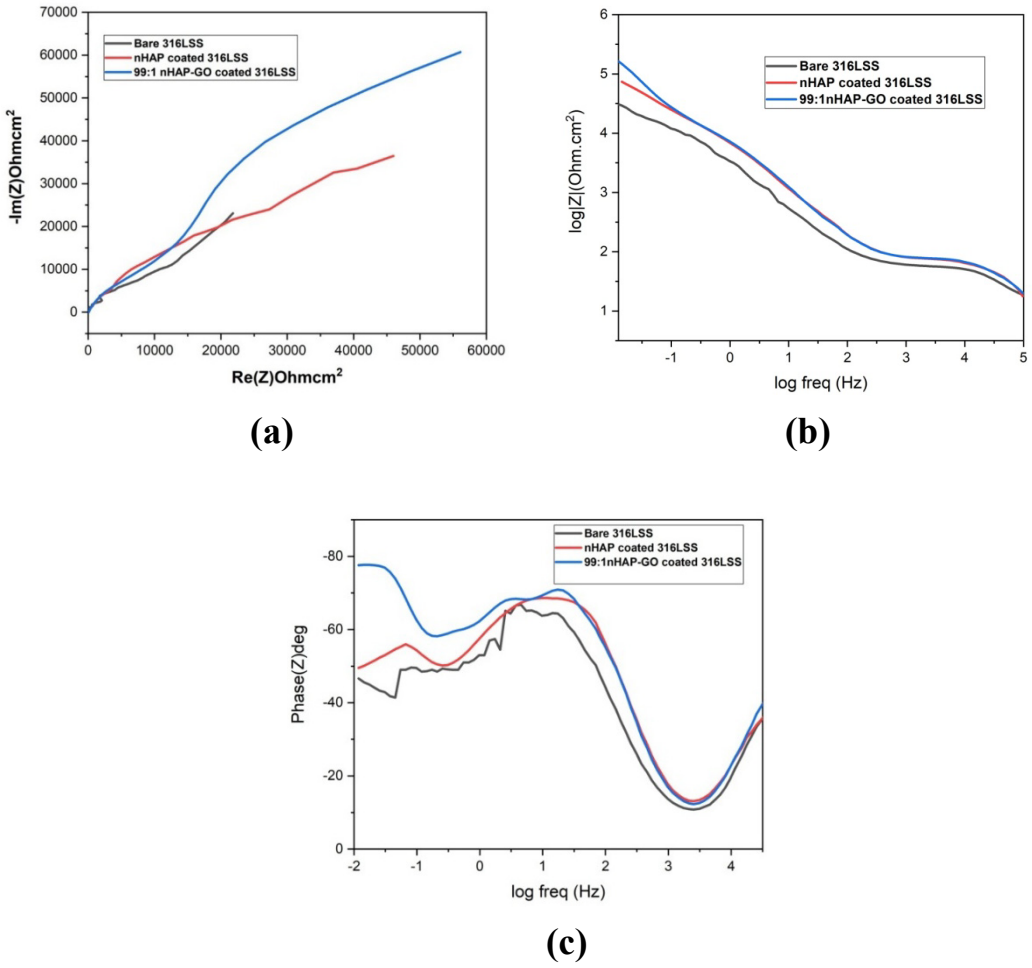


Figure 5. **(a)** Nyquist **(b)** Bode impedance **(c)** Bode phase angle plots for bare 316LSS, nHAP and 99:1 nHAP-GO composite-coated 316LSS.

Table 1. Electrochemical impedance parameters for bare and coated 316LSS

Sample I.D	|Z|	R_s	Q	n	R_1	C	R_2
Bare 316LSS	23289	77.64	-	0.8597	-	0.0001143	4.177×10^{4}
nHAP 316LSS	36468	59.74	4.462×10^{-5}	0.7732	4.256×10^{4}	2.954×10^{-5}	4.256×10^{4}
99:1nHAP-GO 316LSS	60831	57.84	2.803×10^{-5}	0.7214	1.551×10^{5}	9.476×10^{-7}	1.551×10^{5}

of coated samples were higher when compared to bare 316L SS, and the coated samples also possess a higher phase angle. Bode impedance values for bare, nHAP and 99:1 nHAP-GO-coated 316LSS were obtained as 4.49 Ω,4.864 Ω, and 5.195 Ω. Bode phase angles for bare, nHAP and 99:1 nHAP-GO-coated 316LSS were obtained as $-45.8^{0,}$ -49^{0} and -77^{0}.

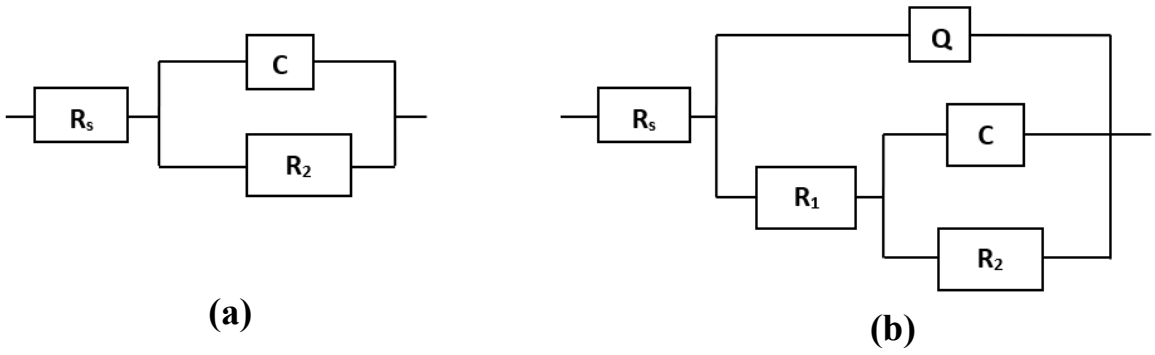


Figure 6. Equivalent circuit for **(a)** Bare 316LSS and **(b)** nHAP- and nHAP-GO-coated 316LSS.

Table 2. Parameters and results for the Tafel plot

Sample I.D	E_{corr}	I_{corr}
Bare 316LSS	-195.780 mV	0.984 µA
nHAP-coated 316LSS	-175.713 mV	0.952 µA
99:1 nHAP-GO coated 316LSS	-88.226 mV	0.910 µA

Potentiodynamic polarisation studies were conducted, and the resulting Tafel plot was generated. From the Tafel fit analysis, performed using ZSimpwin software, the E_{corr} and I_{corr} values for bare and coated samples were determined. For superior corrosion resistivity, the E_{corr} should be high, and the I_{corr} values should be low. Based on the values presented in Table 2, it is clear that the coated samples exhibit enhanced corrosion resistance

From potentiodynamic polarisation studies, a Tafel plot was plotted, which is shown in Figure 7. From the Tafel fit analysis obtained by fitting in ZSimpwin software E_{corr} and I_{corr} values for bare and coated samples were found. E_{corr} should be high, and I_{corr} values have to be low for good corrosion resistivity. From the values given in Table 2, it is evident that coated samples possess more corrosion resistance[27].

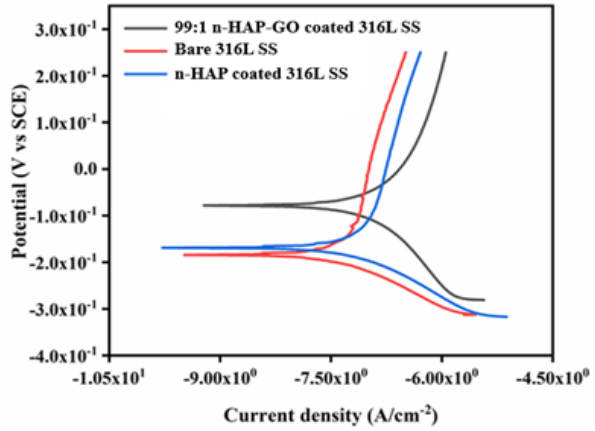


Figure 7. Tafel plot for bare and coated 316LSS

4. Conclusion

In the above work, nHAP, GO and nHAP-GO composites were prepared and uniformly coated on 316LSS by electrophoretic deposition. The presence of functional groups was confirmed by FTIR, and XRD analysis confirmed that the synthesised samples were pure and crystalline in nature. The uniform nature of the deposits and surface roughness was observed with AFM images recorded on the coated samples. The presence of surface roughness in the developed composite coatings indicates that they are promising osseointegration surfaces for new bone formation.

OCP values for the composite-coated sample have moved towards the positive region compared to bare and nHAP-coated 316LSS. Also, composite coatings have higher impedance and resistance values but low capacitance values compared to the bare and nHAP-coated 316LSS. Tafel fitting values also prove that 316LSS coated with composites has higher corrosion resistance. From the above findings, it is clearly evident that the composite-coated implant is better suited to be used as orthopaedic implants.

5. References

1. Pathote D, Kumari P, Singh V, Jaiswal D, Gautam RK, Behera CK. Biocompatibility evaluation, wettability, and scratch behavior of Ta-coated 316L stainless steel by DC magnetron sputtering for the orthopedic applications. Surf Coat Technol. 2023; 459:129392. https://doi.org/10.1016/j.surfcoat.2023.129392
2. Logesh M, Marimuthu A, Ferreira JM, Ramakrishnan P, Ballamurugan AM. Evaluation of the protective nature of GO-BCP nanocomposite coatings on 316L SS in artificial body fluid. J Am Ceram Soc. 2023; 106(6):3843-3852. https://doi.org/10.1111/jace.18975
3. Manovasuki J, Aruna K, George RP, Sridhar TM, Kamachi Mudali U. Graphene oxide hybrid coatings on implant alloys for biomedical applications. In A treatise on corrosion science, engineering and technology. 2022; p. 537-557. Singapore: Springer Nature Singapore. https://doi.org/10.1007/978-981-16-9302-1_27
4. Milan BD, Mohammadzadeh H, Jafari R, Soltani M. A review on hydroxyapatite and its composite coatings on 316L stainless steel substrate for tissue engineering applications.
5. Sasireka A, Renji R, Raj RM, Vignesh S, Raj V, Ashraf IM, Shkir M. Exploration on *in vitro* bioactivity, antibacterial activity and corrosion behavior of strontium-doped hydroxyapatite-reinforced chitosan-polypyrrole/ TNT for bone regeneration. Inorg Chem Commun. 2022; 142:109621. https://doi.org/10.1016/j.inoche.2022.109621
6. Guo Y, Xu Z, Wang Q, Zu S, Liu M, Yu Z, Zhang Z, Ren L. Corrosion resistance and biocompatibility of graphene oxide coating on the surface of the additively manufactured NiTi alloy. Prog Org Coat. 2022; 164:106722. https://doi.org/10.1016/j.porgcoat.2022.106722
7. Ahmad K, Manzur J, Tahir M, Hussain R, Khan M, Wadood A, Avcu E, Rehman MA. Electrophoretic deposition, microstructure and selected properties of zein/cloves coatings on 316L stainless steel. Prog Org Coat. 2023; 176:107407. https://doi.org/10.1016/j.porgcoat.2023.107407
8. Vaez S, Emadi R, Sadeghzade S, Salimijazi H, Kharaziha M. Electrophoretic deposition of chitosan-reinforced baghdadite ceramic nanoparticles on the stainless steel 316L substrate to improve biological and physical characteristics. Mater Chem Phys. 2022; 282:125991. https://doi.org/10.1016/j.matchemphys.2022.125991
9. Dai D, Zhou D, Xie H, Wang J, Zhang C. The design, construction and application of graphene family composite nanocoating on dental metal surface. Biomater Adv. 2022; 140:213087. https://doi.org/10.1016/j.bioadv.2022.213087 PMid:36029723.
10. Raji R, Elangomannan S, Subramani R, Louis K, Periasamy M, Dhanaraj G. Calotropis gigantea fibre- a biogenic reinforcement material for europium substituted hydroxyapatite/poly (3, 4-propylenedioxythiophene) matrix: A novel ternary composite for biomedical applications. ACS Omega. 2022; 7(7):6024. https://doi.org/10.1021/acsomega.1c06372 PMid:35224363 PMCID: PMC8867816.
11. Sivaraj D, Vijayalakshmi K. Novel synthesis of bioactive hydroxyapatite/f-multiwalled carbon nanotube composite coating on 316L SS implant for substantial corrosion resistance and antibacterial activity. J Alloys Compd. 2019; 777:1340-1346. https://doi.org/10.1016/j.jallcom.2018.10.341
12. Jain H, Gupta G, Mondal DP, Pandey A. An effective process to reinforced open cell 316LSS foams with MWCNT for improving biocompatibility. Mater Chem Phys. 2022; 288:126353. https://doi.org/10.1016/j.matchemphys.2022.126353
13. Ji X, Luo C, Jin J, Zhang Y, Sun Y, Fu L. Tribocorrosion performance of 316L stainless steel enhanced by laser-clad 2-layer coating using Fe-based amorphous powder. J Mater Res Technol. 2022; 17:612-621. https://doi.org/10.1016/j.jmrt.2022.01.046
14. Vignesh R, Velusamy B, Nellaiappan SN, Sridhar TM. Tailoring graphene oxide-infused hydroxyapatite coatings on titanium: Electrochemical insights and

simulation for enhanced bone implant performance. ACS Omega. 2025; 10(48):58084.

15. Stango SA, Vijayalakshmi U. Electrochemical deposition of HAP/f-MWCNTs and HAP/GO composite layers on 316L SS implant with excellent corrosion resistance performance. Mater Lett. 2021; 304:130666. https://doi.org/10.1016/j.matlet.2021.130666
16. Aruna K, Vignesh R, Veerabadran KM, Sridhar TM. Corrosion evaluation of nanohydroxyapatite-graphene oxide biocomposite coatings. CORCON; 2022. p. 20.
17. Vignesh R, Aruna K, Balasubramani V, Kumaresan M, Ramar M, Sridhar TM. Electrophoretic deposition of Sr-decorated n-HAP smart coatings on 316L stainless steel: Synergistic corrosion and antibacterial performance for implant applications. Surf Interfaces. 2026; 109846. https://doi.org/10.1016/j.surfin.2026.109846
18. Lin FH, Hsu YS, Lin SH, Sun JS. The effect of Ca/P concentration and temperature of simulated body fluid on the growth of hydroxyapatite coating on alkali-treated 316L stainless steel. Biomaterials. 2002; 23(19):4029-4038. https://doi.org/10.1016/S0142-9612(02)00154-0 PMid:12162336.
19. Vafa E, Bazargan-Lari R, Bahrololoom ME. Electrophoretic deposition of polyvinyl alcohol/natural chitosan/bioactive glass composite coatings on 316L stainless steel for biomedical application. Prog Org Coat. 2021; 151:106059. https://doi.org/10.1016/j.porgcoat.2020.106059
20. Mahmoudi M, Farhadian M, Raeissi K, Labbaf S, Karimzadeh F, Golozar MA, Barnoush A. The role of graphene oxide interlayer on corrosion barrier and bioactive properties of electrophoretically deposited ZrO_2-10 at% SiO_2 composite coating on 316 L stainless steel. Mater Sci Eng C. 2020; 117:111342. https://doi.org/10.1016/j.msec.2020.111342 PMid:32919689.
21. Li M, Liu Q, Jia Z, Xu X, Shi Y, Cheng Y, Zheng Y, Xi T, Wei S. Electrophoretic deposition and electrochemical behavior of novel graphene oxide-hyaluronic acid-hydroxyapatite nanocomposite coatings. Applied Surface Science. 2013; 284:804-810. https://doi.org/10.1016/j.apsusc.2013.08.012
22. Han W, Liu L, Yu B, Zhu Q. Electrodeposition of graphene oxide-hydroxyapatite composite coating on titanium substrate. Ceram Int. 2023; 49(6):9647-9656. https://doi.org/10.1016/j.ceramint.2022.11.135
23. Gopi D, Ramya S, Rajeswari D, Kavitha L. Corrosion protection performance of porous strontium hydroxyapatite coating on polypyrrole-coated 316L stainless steel. Colloids Surf B: Biointerfaces. 2013; 107:130-136. https://doi.org/10.1016/j.colsurfb.2013.01.065 PMid:23475060.
24. Ahmed Y, Yasir M, Ur Rehman MA. Fabrication and characterization of zein/ hydroxyapatite composite coatings for biomedical applications. Surfaces. 2020; 3(2):18. https://doi.org/10.3390/surfaces3020018
25. Khosravi F, Nouri Khorasani S, Rezvani Ghomi E, Kichi MK, Zilouei H, Farhadian M, Esmaeely Neisiany R. A bilayer GO/nanofibrous biocomposite coating to enhance 316L stainless steel corrosion performance. Mater Res Express. 2019; 6(8):086470. https://doi.org/10.1088/2053-1591/ab26d5
26. Kaviya M, Ramakrishnan P, Mohamed SB, Ramakrishnan R, Gimbun J, Veerabadran KM, Kuppusamy MR, Kaviyarasu K, Sridhar TM. Synthesis and characterization of nano-hydroxyapatite/graphene oxide composite materials for medical implant coating applications. Mater Today: Proceedings. 2021; 36:204-207. https://doi.org/10.1016/j.matpr.2020.02.932
27. Mohandoss S, Ganeasan MS, Manovasuki J, Sridhar TM. Surface modification of 316L stainless steel dental implants by novel bioinert nano zirconia coating. Trends Biomater Artif Organs. 2020; 34(3):100.

Author Contributions

K. Aruna - Conceptualization, Investigation, Methodology, Writing – Original Draft, R. Vignesh - Data curation, formal analysis and review & editing, P.V. Benisha– Data curation and formal analysis, T.M. Sridhar - Formal analysis, Supervision, Validation, Writing – Review & Editing.